Genome Medicine

RESEARCH

Open Access

Chromatin conformation capture in the clinic: 4C-seq/HiC distinguishes pathogenic from neutral duplications at the *GPR101* locus

Adrian F. Daly[1†], Leslie A. Dunnington[2,3], David F. Rodriguez-Buritica[2,3], Erica Spiegel[4], Francesco Brancati[5,13], Giovanna Mantovani[6,7], Vandana M. Rawal[8], Fabio Rueda Faucz[9], Hadia Hijazi[10], Jean-Hubert Caberg[11], Anna Maria Nardone[12], Mario Bengala[12], Paola Fortugno[13,14], Giulia Del Sindaco[6,7], Marta Ragonese[15], Helen Gould[16], Salvatore Cannavò[15], Patrick Pétrossians[1], Andrea Lania[17,18], James R. Lupski[10,19,20,21], Albert Beckers[1], Constantine A. Stratakis[9,22,23], Brynn Levy[24], Giampaolo Trivellin[17,18*†] and Martin Franke[25*†]

Abstract

Background X-linked acrogigantism (X-LAG; MIM: 300942) is a severe form of pituitary gigantism caused by chromosome Xq26.3 duplications involving *GPR101*. X-LAG-associated duplications disrupt the integrity of the topologically associating domain (TAD) containing *GPR101* and lead to the formation of a neo-TAD that drives pituitary *GPR101* misexpression and gigantism. As X-LAG is fully penetrant and heritable, duplications involving *GPR101* identified on prenatal screening studies, like amniocentesis, can pose an interpretation challenge for medical geneticists and raise important concerns for patients and families. Therefore, providing robust information on the functional genomic impact of such duplications has important research and clinical value with respect to gene regulation and triplosensitivity traits.

Methods We employed 4C/HiC-seq as a clinical tool to determine the functional impact of incidentally discovered *GPR101* duplications on TAD integrity in three families. After defining duplications and breakpoints around *GPR101* by clinical-grade and high-density aCGH, we constructed 4C/HiC chromatin contact maps for our study population and compared them with normal and active (X-LAG) controls.

Results We showed that duplications involving *GPR101* that preserved the centromeric invariant TAD boundary did not generate a pathogenic neo-TAD and that ectopic enhancers were not adopted. This allowed us to discount presumptive/suspected X-LAG diagnoses and *GPR101* misexpression, obviating the need for intensive clinical follow-up.

†Adrian F. Daly, Giampaolo Trivellin and Martin Franke contributed equally to this work.

*Correspondence:
Giampaolo Trivellin
giampaolo.trivellin@hunimed.eu
Martin Franke
mfra2@upo.es
Full list of author information is available at the end of the article

Conclusions This study highlights the importance of TAD boundaries and chromatin interactions in determining the functional impact of copy number variants and provides proof-of-concept for using 4C/HiC-seq as a clinical tool to acquire crucial information for genetic counseling and to support clinical decision-making in cases of suspected TADopathies.

Keywords GPR101, Topologically associating domains, Neo-TAD, X-linked acrogigantism, Pituitary tumor, Prenatal diagnosis, Chromosome microarray, 4C, HiC, Enhancer

Background

Chromatin is folded within the nucleus in an organized three-dimensional fashion that permits interactions for the purpose of gene regulation and expression [1]. Topologically associating domains (TADs) are a key organizational element in this dynamic regulatory architecture and are considered a basic component of genome organization [2]. TADs are sub-megabase scale regions that have high levels of internal interactions among genes and regulatory elements and are insulated from interactions with nearby sequences by TAD boundaries. These boundaries are characterized by the presence of specific proteins including CCCTC-binding factor (CTCF) and other regulators of chromatin structure and activity, such as cohesin and its associated proteins [3, 4]. Within TADs, interactions take place between promoters and enhancers via chromatin loop formation. The importance of these mechanisms for genomic regulation is underlined by the fact that TADs and their boundaries are commonly conserved across species, while single nucleotide variants, epigenetic inactivation at boundaries elements or genomic disruption of TAD boundaries significantly affect gene expression [1, 5, 6]. Duplications, deletions, and inversions can disrupt TAD boundaries and alter gene regulation within the TAD by placing promoters under the control of ectopic enhancers, for example, by fusing two flanking TADs or by forming a neo-TAD [7, 8]. In medicine, a growing number of genomic disorders ("TADopathies") are now recognized to be driven by TAD disruption [9]. TADopathies described to date include congenital limb malformations, neurological and retinal diseases, and various solid and hematological malignancies [10–15].

Among the TADopathies, we have focused on the characterization and investigation of X-linked acrogigantism (X-LAG) [16]. X-LAG is a rare and severe form of pituitary gigantism, in which infants develop mixed growth hormone (GH)- and prolactin-secreting pituitary macroadenomas (also known as pituitary neuroendocrine tumors or PitNETs) [17]. Individuals with X-LAG have small duplications—on average 600 kb in size—at chromosome Xq26.3 involving the *GPR101* gene. This gene encodes an orphan G protein-coupled receptor (GPCR) that in silico, in vitro, and in vivo studies have shown to be highly constitutively active [17–22]. X-LAG can occur sporadically as constitutional or somatic mosaic cases or as an X-linked dominant inherited disorder [17, 23–26]. Normally *GPR101* sits alone in its own TAD and is insulated from nearby enhancers by a centromeric, tissue-invariant TAD boundary [16]. In X-LAG, duplications lead to the loss of this border and local sequences are rearranged within a neo-TAD that places the *GPR101* promoter under the control of ectopic enhancers. This has the effect of driving massive (> 1000-fold) overexpression of *GPR101* in anterior pituitary cells, where its constitutive activity causes GH hypersecretion and leads to the pituitary gigantism phenotype [18, 20].

As X-LAG is the only disease currently associated with *GPR101* and is X-linked dominant and fully penetrant, individuals carrying *GPR101* duplications that were identified during routine genetic testing may reasonably be flagged as potentially having X-LAG. This can be a source of considerable anxiety owing to the severity of the gigantism phenotype and the challenging treatments that are needed for disease control [24, 27].

Chromatin conformation capture-derived techniques like 4C-seq and HiC are the methodological workhorses for the study of TADs [28]. Until now, they have largely been used in the setting of fundamental and translational research and have not been applied widely to clinical diagnostics. We employed 4C-seq and HiC to study individuals with *GPR101* duplications encountered during routine genetic practice, or those with an X-LAG-like clinical presentation but indeterminate array comparative genomic hybridization (aCGH) results. These 4C-seq/HiC results allowed us to refine clinical diagnoses and rule out X-LAG by showing that *GPR101* duplications that preserve the invariant TAD border do not permit the formation of a pathogenic neo-TAD.

Methods

Study population

The study population consisted of the following individuals: in family 1, the propositus (F1A) and her mother (F1B) and father (F1C); in family 2, the propositus F2A; in family 3, the propositus F3A; and the sporadic case, SC1. All presented clinically as described below. All underwent 4C-seq, while F2A and SC1 also underwent

HiC analysis. For 4Cseq, the normal controls were F1B and F1C and three unaffected individuals from the GEO database under the accession code GSE193114 [16, 29, 30]. The population of X-LAG subjects consisted of six affected females (S2, S6, S7, S9, S13, and S17; age at disease onset: 3–48 months) that were recruited under clinical protocols 97-CH-0076 (NIH; ClinicalTrials.gov: NCT00001595) and B707201420418 (University of Liège), as outlined previously [16, 29]. The 4C-seq and HiC datasets included in the current study are available at [29, 30].

Family 1

Individual F1A was identified prenatally following a routine amniocentesis that was performed in her 36-year-old mother (G2P1) following prenatal counseling for advanced maternal age. Neither her parents nor their families had a history of overgrowth, endocrine, or other abnormalities. Her 3-year-old sister was of normal size and had met her developmental milestones. In F1A, early intrauterine growth had been restricted due to placenta previa and there was a persistent right umbilical vein. Chromosome microarray analysis (CMA) on a SNP Cytoscan HD platform showed the presence of a small microduplication of ~ 64 kb on chromosome Xq26.3 involving the region 136,068,349–136,131,892 (hg19) that included *GPR101*. Neither of the parents shared this duplication on follow-up examination by qPCR. The pregnancy progressed uneventfully. At birth (39 week; C-section), she weighed 2.89 kg (10th percentile; − 1.29 SD), was 48.26 cm in length (17th percentile; − 0.95 SD), and she had a head circumference of 33.3 cm (15th percentile; − 1.02 SD). She had no dysmorphic features. Due to the CMA finding of a duplication involving *GPR101*, a presumptive potential diagnosis of X-LAG was made. Initial hormonal testing in the early neonatal period revealed elevated GH, insulin-like growth factor-1 (IGF-1), and prolactin levels. Over the course of her first 6 months of life, regular hormonal testing and growth measurements were performed. By 3 months of age, GH, IGF-1, and prolactin normalized, while her height (− 0.17 SD) and weight (+ 0.08 SD) were unremarkable. She underwent regular follow-up with community pediatricians and pediatric endocrinologists over the next 2 years. Her hormonal levels remained normal and she met all her developmental milestones appropriately. These clinical findings were inconsistent with an X-LAG diagnosis.

Family 2

Individual F2A, a healthy adult female, came to light during her first pregnancy. During routine ultrasound screening, multiple fetal abnormalities were noted, including a lymphatic malformation in the neck, dilated cardiac ventricles, and growth restriction. Following genetic counseling, an amniocentesis was performed. The SNP-CMA (Cytoscan HD platform) revealed a 277-kb duplication on chromosome Xq26.3 involving the region 136,111,060–136,388,326 (hg19); *GPR101* was the only coding gene included in the duplication. Due to fetal malformations, the pregnancy was terminated. There was no family history of endocrine, growth, or other disorders. Individual F2A was found to have the same duplication carried by the fetus on both SNP and exon arrays (Cytoscan HD and XON Arrays). This was separately confirmed in the DNA samples from F2A derived from blood and buccal swabs using a droplet digital PCR (ddPCR) assay (Additional file 1: Fig. S1). The duplication breakpoints were mapped using high-density aCGH (HD-aCGH) and breakpoint-junction PCR. This showed a complex rearrangement at the telomeric end of the duplication within the 3′UTR of *GPR101* junction, which consisted of a duplication-normal sequence-duplication pattern (DUP-NML-DUP) (Additional file 1: Fig. S2). F2A later had a normal pregnancy, and a healthy girl was found not to have the Xq26.3 duplication.

Family 3

Individual F3A was a 42-year-old man with a lifelong history of developmental delay, mild intellectual disability, short stature (< 3rd centile), brachydactyly, EEG abnormalities, bilateral cranial nerve VI dysfunction, horizontal nystagmus, and hyperintensity of the globus pallidus on brain MRI. He also had episodes of psychomotor arrest on electroencephalogram. During workup for a genetic cause, he was found to be a phenotypic male with a 46, XY karyotype, and aCGH showed a 508-kb duplication on chromosome Xq26.3 involving the region 136,028,815–136,536,734 (hg19); *GPR101* was the only coding gene included in the duplication. This copy number gain was independently confirmed using a ddPCR assay (Additional file 1: Fig. S1). His hormonal profile, including pituitary, adrenal, thyroid, and gonadal axes, was normal. His mother had a similar phenotype with mild intellectual disability, EEG abnormalities, short stature (< 3rd centile), brachydactyly, and globus pallidus hyperintensity and also had the same Xq26.3 duplication. A younger sister who was affected by short stature (< 3rd centile), brachydactyly, intellectual disability, and EEG abnormalities, but with normal brain imaging, did not carry the Xq26.3 duplication. Therefore, the duplication did not segregate with the phenotype in the family. Another younger sister was of normal phenotype, had two normal children, and did not carry the Xq26.3 duplication.

To explore the functional effects of the duplications seen in F1-F3 and their roles as potential contributors to clinical phenotypes or as neutral effects, we studied chromatin contacts at the X-LAG locus using 4C-seq and HiC. We then compared these profiles to normal controls.

Sporadic case 1 (SC1)

Individual SC1 developed overgrowth beginning within the first 6 months of life. There was no family history of endocrine or growth disorders and her mean parental height was 158.5 cm. From the age of two, her growth curve rapidly diverged, and she developed worsening gigantism, measuring 130 cm in height by 3 years of age (height *z*-score > +8 SD). She was diagnosed with GH and IGF-1 excess due to a pituitary macroadenoma at the age of four. She was resistant to treatment with the first-generation somatostatin analog, octreotide, and then underwent neurosurgical resection of her pituitary adenoma. Disease control was achieved by her mid-teens, but she developed permanent gigantism and her final adult height was 184 cm (+2.92 SD; +25.5 cm above mean parental height; Additional file 1: Fig. S3). Screening for known germline genetic causes of pituitary gigantism including the genes *AIP*, *MEN1*, and *CDKN1B* was negative. As part of the discovery cohort studies for X-LAG, on clinical-grade aCGH she did not have any copy number change in the region of interest at the X-LAG locus [17]. No copy number changes involving *GPR101* or other genes in the X-LAG locus were found on HD-aCGH. aCGH of her pituitary tumor DNA did not show any evidence of *GPR101* duplication (data not shown). In SC1, even following extensive investigations, uncertainty remained whether the infant-onset pituitary gigantism was due to X-LAG or if she was a phenocopy. To assist in making/excluding a definitive clinical diagnosis, we examined *GPR101* and the X-LAG locus by performing HiC and we compared the results to those obtained in individuals with X-LAG.

Clinical grade aCGH and HD-aCGH

Subjects underwent genetic diagnosis by testing peripheral blood DNA using clinical-grade aCGH and research-based HD-aCGH with high-density probes tiling the critical region within Xq26.3 (chrX:135,001,882–136,499,429, hg19). Breakpoint junction analysis was performed using long-range PCR followed by Sanger sequencing of the PCR products. Both methods were previously described in detail [17].

Copy number variant (CNV) analysis

CNV assays were performed by employing four TaqMan hydrolysis probes consisting of a pair of unlabeled primers and a FAM-labeled Minor Groove Binder (MGB) probe. The assays employed were specific for the following genes: *RBMX* (Hs02426405_cn), *GPR101* (Hs01730605_cn and Hs01818174_cn), and *ZIC3* (Hs02692150_cn). The VIC-labeled *RPP30* (*Rnase P*) assay (4403326, Thermo Fisher Scientific) was used as an internal control. All assays were supplied from Thermo Fisher Scientific (Waltham, MA, USA) and were used in conjunction with a ddPCR instrument (QX200 Droplet Digital PCR System, Bio-Rad, CA, USA). The ddPCR assays were performed according to the manufacturer's protocol. Briefly, experiments were prepared in 96 microwell plates and consisted of 22 µl reactions containing 20 ng of blood-derived genomic DNA, 11 µl 2X ddPCR Supermix for Probes (no dUTP, #1863024, Bio-Rad), and 1.1 µl each of one target gene and reference CNV assay mixes. Data were analyzed using the QuantaSoft analysis software (version 1.7.4.0917). Results are displayed as copy number data and Poisson-based 95% confidence intervals (CI). The copy number was determined by the relative relationship between the quantity of the target gene and the reference gene.

4C-seq/HiC sample preparation

Cells from cultured peripheral blood mononuclear cells (PBMCs) were prepared for chromatin fixation and nuclei extraction following the protocol we described in [16]. Approximately 2.5×10^6 fixed and isolated nuclei were snap-frozen in liquid nitrogen and used as input for HiC and 4C-seq. Experiments were conducted as singletons.

4C-seq library preparation

3C and 4C library preparation was performed as previously described [16], including detailed information about 4C-seq primer sequences for the *GPR101* viewpoint, viewpoint fragment coordinates, and corresponding digestion strategies for primary and secondary restriction enzymes. 4C-seq libraries were multiplexed, employing Illumina TrueSeq adapters, and sequenced utilizing DNBseq technology to generate 100-bp single-end reads, yielding approximately 10 million raw sequencing reads per sample.

4C-seq data analysis and visualization

4C-seq read mapping to the human genome (GRCh37/hg19) and read filtering were performed as previously described [31]. Mapped reads were converted to read counts per restriction fragment of the first restriction enzyme. For visualization, all 4C-seq profiles were normalized for reads per million within the specified genomic region (chrX:135,000,000–137,000,000, hg19) and subjected to signal smoothing using a 10-fragment running window. To compare 4C interaction profiles

between subjects and family controls, the normalized read counts of controls were subtracted from the subject signal. Matched controls were used for signal subtraction to control batch effects between experiments. F1A and F2A were compared to the family controls, F1B and F1C, while F3A was compared to unaffected controls retrieved from the GEO database under the accession code GSE193114 [16, 29, 30]. The resulting bedgraph files were visualized using the UCSC Genome Browser, focusing on the genomic target region (chrX:135,336,766–136,561,684, hg19) in Fig. 1 and Additional file 1: Fig. S5.

For the comparative analysis shown in the heatmap in Fig. 2, normalized and subtracted 4C-seq signals (subjects vs. controls) were visualized using ggplot2 [32] with genomic positions binned in 50-kb increments on the x-axis along the target region. The average score was represented using the Viridis color palette. For comparisons with 4C-seq data from X-LAG subjects, we used data from affected subjects S6, S9, S13, S7, S2, and S17, and three unaffected control subjects, as described in previous studies [16]. Data on these X-LAG subjects and controls were retrieved from the GEO database under accession code GSE193114 [29].

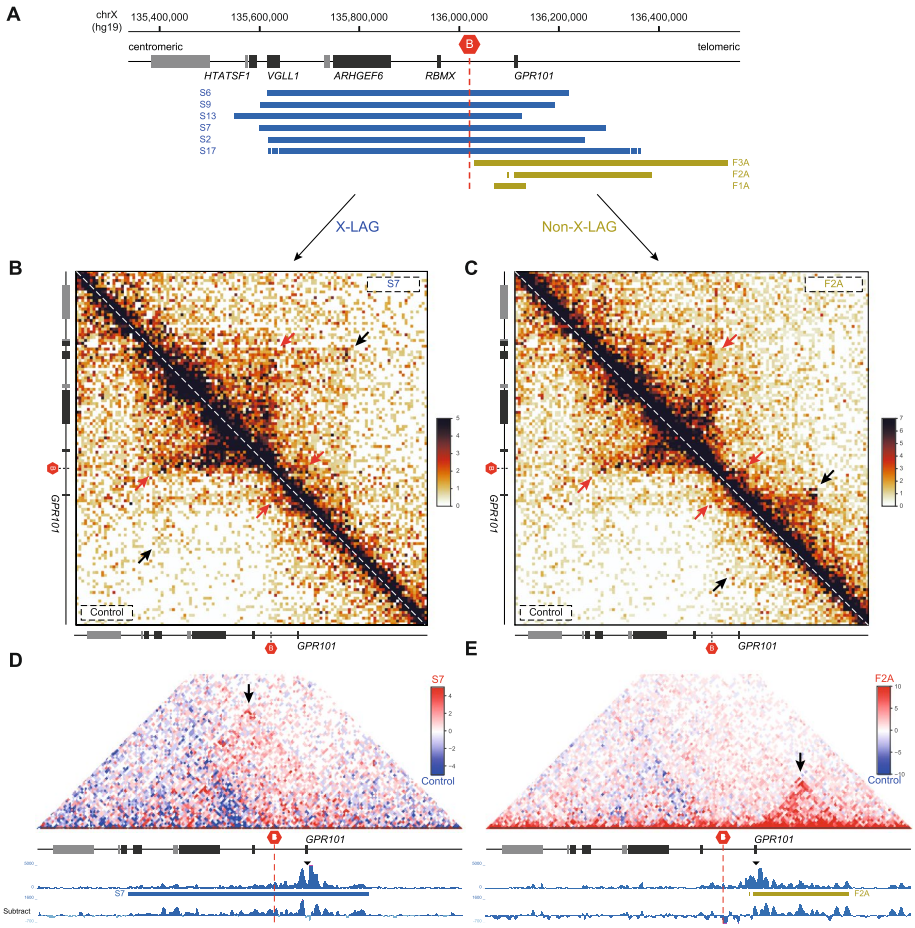

Fig. 1 Impact of inter- and intra-TAD duplications on chromatin organization at the X-LAG locus. **A** Schematic representation of the extended X-LAG locus (hg19, chrX:135,336,766–136,561,684), delineating the genomic position of an invariant TAD border (red hexagon). Below, the position of partially overlapping tandem duplications involving *GPR101* from subjects with X-LAG (highlighted by blue boxes) [16] that traverse the TAD border (inter-TAD duplications), alongside duplications from subjects of the current study (yellow boxes) that remain within TAD boundaries (intra-TAD duplications). **B** and **C** HiC at the X-LAG locus, showing normalized contact matrices at 10-kb resolution from the X-LAG subject S7 and non-X-LAG subject F2A in a side-by-side comparison to controls. Normal TAD configuration at the locus is highlighted by red arrows. Additional chromatin interactions, induced by inter- and intra-TAD duplications, are denoted by black arrows. HiC difference maps relative to controls (**D** and **E**) depict the increase in chromatin interactions (black arrows) in subject S7 and F2A. Below, corresponding 4C-seq profiles originating from the *GPR101* viewpoint (black triangle) are displayed, alongside the genomic position of the duplication and the subtraction profiles relative to control samples. Inter-TAD duplications in X-LAG (**B** and **D**) result in increased chromatin interaction of *GPR101* with regions centromeric of the TAD border (neo-TAD formation). Intra-TAD duplications, confined to *GPR101* and excluding the invariant TAD border (**C** and **E**), exhibit increased telomeric chromatin interactions

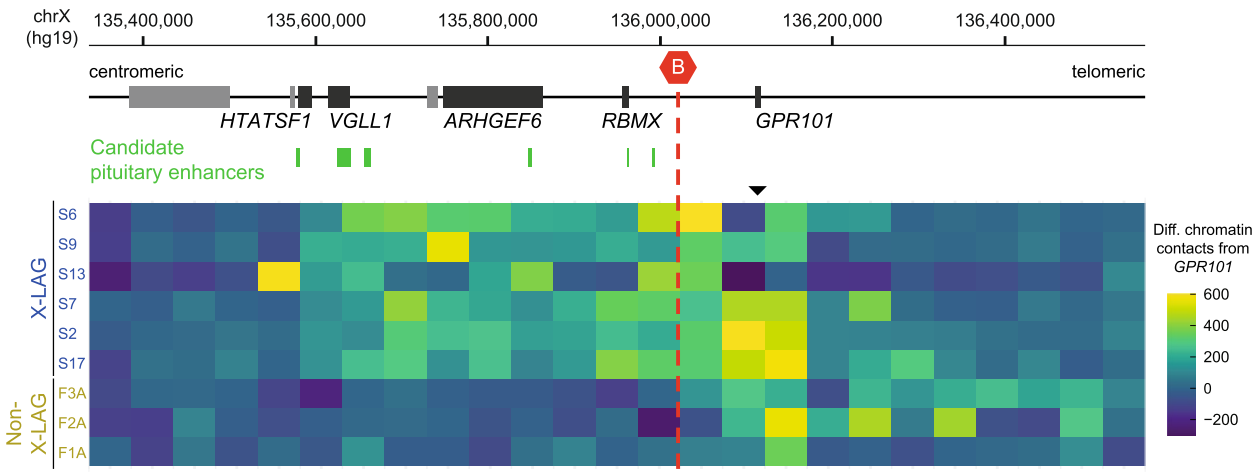

Fig. 2 Modulation of *GPR101* chromatin interactions by inter- and intra-TAD duplications. Schematic representation of the extended X-LAG locus (hg19, chrX:135,336,766–136,561,684), delineating the genomic positions of putative pituitary enhancers (green boxes) and an invariant TAD border (red hexagon), which separates *GPR101* from pituitary activity in normal conditions. Below, heatmap showing differential chromatin contacts at a 50-kb genomic bin size in X-LAG and non-X-LAG subject samples compared to controls, as inferred from 4C-seq experiments with a viewpoint located at the *GPR101* promoter. The genomic bin containing the viewpoint is indicated by a black arrowhead. All X-LAG subjects exhibit similar patterns of ectopic chromatin interactions from *GPR101* with the centromeric region containing putative pituitary enhancers. This pattern is absent in non-X-LAG subjects. The 4C-seq data from X-LAG subjects S6, S9, S13, S7, S2, and S17 and their respective controls (described in Franke et al. [16]) were retrieved from the GEO database under accession code GSE193114 [29]

Quantification of GPR101 chromatin contacts with enhancer regions

4C-seq normalized read counts for restriction fragments overlapping with candidate enhancer regions that we previously identified (eVGLL1-intronic, chrX:135,625,877–135,641,072; eVGLL1-distal, chrX:135,656,769–135,660,247; eARHGEF6-intronic, chrX:135,846,959–135,851,769; eRBMX, chrX:135,959,959–135,963,959; eAK055694, chrX:135,990,759–135,994,160) were extracted from the *GPR101* viewpoint for three groups: subjects with duplications causing X-LAG (S6, S9, S13, S7, S17, S2) retrieved from the GEO database under accession code GSE193114 [29]; subjects with duplications but without X-LAG described in the current study (F1A, F2A, F3A); and control samples (F1B, F1C from the current study, and Control_S13, Control_S2_S7, Control_S9) [16, 29, 30].

To systematically identify PCR bias for spurious and high read counts in single fragments, a *Z*-score was calculated for each fragment count to determine how many standard deviations the value was from the mean (a) within the candidate region of each sample and (b) across the same restriction fragment between all samples. A *Z*-score threshold of ± 3 was established to identify extreme variations. Values with *Z*-scores beyond this threshold were flagged as outliers and omitted from further analysis. Total read count in each candidate region was averaged and displayed as a box plot showing the distribution of read counts across the X-LAG, the duplication but non-X-LAG, and control sample groups.

For statistical analysis, comparisons between groups (X-LAG dup vs. control; non-X-LAG dup vs. control; X-LAG dup vs. non-X-LAG dup) were performed using a non-parametric Wilcoxon rank-sum exact test (two-sided, 95% confidence interval). The Wilcoxon rank-sum test was chosen due to its ability to handle non-normally distributed data and small sample sizes. All statistical analyses were conducted using R version 4.0.3 (2020–10-10).

HiC library preparation

Nuclei isolated from subjects and controls were processed for 3C and HiC library construction following a previously described protocol [33] with minor modifications detailed in [34]. Final HiC libraries were multiplexed and sequenced using DNBseq technology, resulting in 100-bp paired-end reads, with approximately 400 million raw sequencing read pairs generated for each sample.

HiC data analysis and visualization

HiC data analysis was performed as previously described with minor modifications [34]. Briefly, HiC paired-end reads were mapped to the human genome (GRCh37/hg19) using BWA [35]. Hi-C pairs representing valid ligation events were filtered, and PCR duplicates were removed using the pairtools package (https://github.com/mirnylab/pairtools). Unligated fragments and self-ligation events (dangling and extra-dangling ends,

respectively) were filtered out by excluding paired-reads mapping to the same or adjacent restriction fragments. The resulting filtered pairs file was converted to a TSV (tab-separated values) file, serving as input for Juicer Tools 1.13.02 Pre to generate multiresolution HiC files [36]. Specifically, the analysis utilized custom scripts (https://gitlab.com/rdacemel/hic_ctcf-null): the hic_pipe.py script first generated TSV files with the filtered pairs, followed using the filt2hic.sh script to produce Juicer HiC files.

All HiC visualization was performed using the FAN-C 0.9.23 toolkit within the genomic target region [37]. HiC contact matrices of subjects were visualized in a side-by-side comparison with controls at 10-kb resolution, employing the VC-SQRT (square root vanilla coverage) normalization method. Differences in HiC contact matrices between subject and control samples were visualized at 10-kb resolution using the "-c difference" argument.

Results

When mapped on the X-LAG locus, the duplications in cases F1A, F2A, and F3A had different centromeric breakpoints to those observed in previously characterized individuals with X-LAG (Fig. 1A). Of note, none of the cases F1A, F2A, and F3A had duplications that involved the invariant centromeric boundary of the TAD containing *GPR101*, denoted as a red hexagon in Fig. 1A. To distinguish changes in chromatin interactions at the TAD level at the X-LAG locus, we performed HiC in F2A and compared this with those obtained in normal controls and in individual S7, with proven X-LAG [16]. The neo-TAD formed due to the duplication in individual S7 is clearly seen as compared with control in Fig. 1B (black arrow). In contrast, the HiC map in F2A shows no new interactions in the centromeric direction crossing the invariant boundary (Fig. 1C). The comparison is further underlined in Fig. 1D and E, which depict a neo-TAD in the X-LAG case S7 that is not present in case F2A. New chromatin interactions in F2A are limited by and do not encroach on the invariant centromeric TAD boundary, thereby limiting the *GPR101* duplication to an intra-TAD location.

In the case of SC1, the clinical characteristics were identical to that of established X-LAG individuals but no duplication could be identified within the X-LAG locus on different aCGH platforms. To eliminate the possibility of aberrant chromatin interactions at the X-LAG locus, we conducted an HiC analysis in individual SC1. Comparative analysis with normal controls yielded no discernible differences (Additional file 1: Fig. S4).

Next, we generated 4C-seq contact frequency data of individuals F1A, F2A, and F3A, which showed a clear demarcation from those obtained in proven X-LAG cases (Fig. 1D and E, Additional file 1: Fig. S5). Differential 4C-seq interactions with respect to controls from the *GPR101* viewpoint were plotted as a heatmap and showed that in contrast to the extensive ectopic interactions that characterize neo-TAD formation in X-LAG, this pattern was absent in individuals F1A, F2A, and F3A (Fig. 2). In particular, the duplications in cases F1A, F2A, and F3A did not permit new interactions with the region where the candidate pituitary enhancers are located or with the enhancers themselves (Additional file 1: Fig. S6). Taken together, these results show that duplications that include *GPR101* but that do not include or cross the invariant centromeric *GPR101* TAD boundary do not cause the X-LAG phenotype if they do not induce a neo-TAD that recruits ectopic enhancers.

Discussion

In X-LAG, tandem duplications involving *GPR101* at chromosome Xq26.3 lead to the formation of a neo-TAD that places *GPR101* under the control of ectopic centromeric enhancers that drive overexpression of GPR101 in somatotropes of the anterior pituitary [16]. In all cases of X-LAG described to date, *GPR101* duplications cause disease, and the condition can be inherited in an X-linked dominant manner [38, 39]. In the current study, we addressed a series of clinically derived findings that apparently challenged this link between *GPR101* duplication and pituitary disease.

Using 4C-seq/HiC, we were able to differentiate between duplications involving *GPR101* causing X-LAG and those that were not associated with X-LAG. These results show that a copy number gain involving *GPR101* is, in itself, not sufficient to produce clinical disease. TAD boundary disruption is a necessary step for markedly elevated pituitary *GPR101* misexpression to occur and to cause clinical disease. Duplications that are causative of X-LAG rearrange an invariant boundary and permit the formation of a neo-TAD that adopts enhancers between *RBMX* and *VGLL1*. In cases with a discrete *GPR101* duplication that neither includes neighboring centromeric genes and enhancers nor impacts the integrity of the centromeric invariant *GPR101*-TAD boundary, new chromatin interactions with the pituitary-active ectopic enhancers are not formed. *GPR101*, therefore, is not misexpressed in the pituitary gland and the pituitary gigantism phenotype is absent. The 4C/HiC maps show clearly that these limited duplications were restricted to the intra-TAD region and therefore were incapable of generating a pathogenic neo-TAD. This effectively illustrates the fundamental concept of TAD boundaries as being a critical element in delineating regulatory activities within genomes (Fig. 3). In instances of intra-TAD duplications,

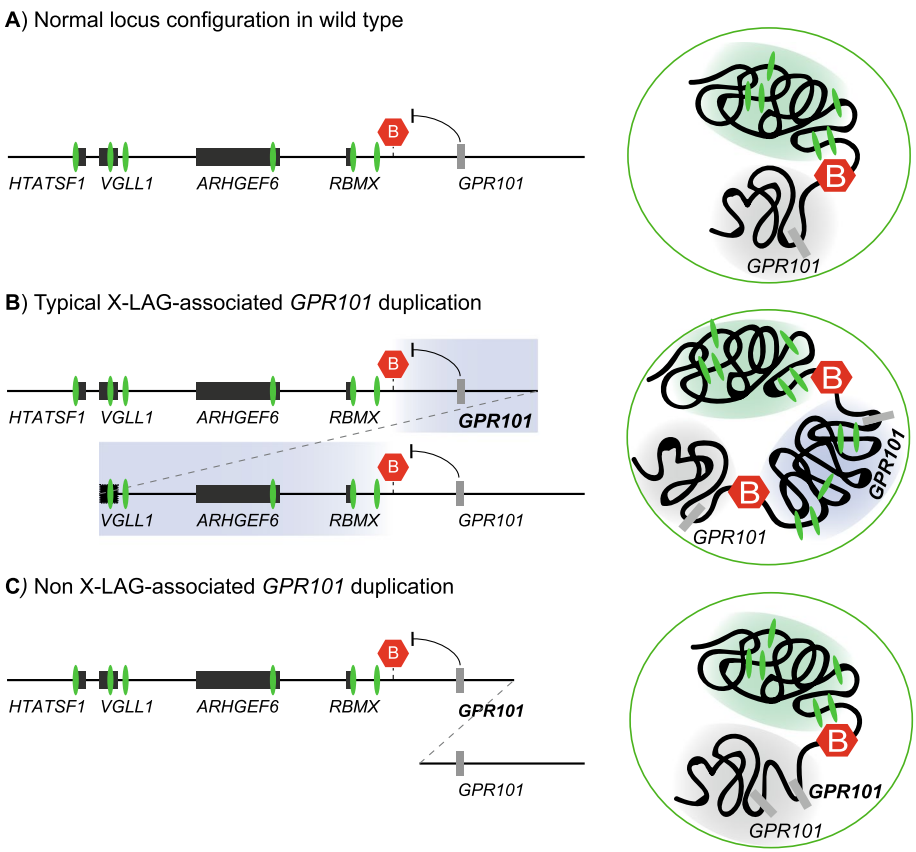

Fig. 3 Disease mechanism induced by inter- and intra-TAD duplications at the X-LAG locus. Schematic illustrating the configuration of TAD boundaries at the X-LAG locus with a linear genomic view (left) and a schematic representation of TAD configuration (right). **A** Under normal conditions, *GPR101* is separated by a TAD boundary (red hexagon) from putative pituitary enhancers (green ovals). **B** Inter-TAD duplications associated with X-LAG, spanning the TAD boundary, lead to the formation of a neo-TAD (blue) that involves ectopic chromatin interactions between *GPR101* and pituitary enhancers, consequently causing GPR101 misexpression and gigantism. **C** Intra-TAD duplications of *GPR101* that "preserve" the TAD boundary do not generate a neo-TAD. As a result, the additional copy of *GPR101* remains segregated from pituitary enhancers. Note that the size and position of duplications are indicated by overlap in the schematic representation

the additional copies (here, *GPR101*) remain insulated by the centromeric TAD boundary, thereby safeguarding it from misexpression. Conversely, the formation of neo-TADs facilitates interactions between pituitary enhancers and *GPR101*. The current study provides new evidence to confirm the crucial role of the neo-TAD containing *GPR101* under ectopic enhancer control in the pathogenesis of X-LAG.

Two of the duplications in question arose in the setting of prenatal genetic testing using CMA. The use of CMA, exome sequencing (ES), and genome sequencing (GS) techniques to investigate fetal abnormalities on ultrasound or in other high-risk pregnancies is growing rapidly. As in all areas of medical genetics, the greater data yield of these methods amplifies the challenges relating to the interpretation and reporting of variants of uncertain significance. When interpreting single nucleotide variants (SNVs) and CNVs, extensive genomic databases and in silico tools exist to aid medical genetic decision-making. For rare SVs and changes affecting non-coding sequences, it is more challenging to predict their pathological impact. Local and national libraries of CMA findings related to clinical data exist, but these libraries can have incomplete data for rare or newly identified genetic diseases. In both cases described here, amniocentesis was performed due to recognized criteria like fetal ultrasound abnormalities or advanced maternal age. CMA analysis revealed small duplications that included *GPR101* and, absent evidence to the contrary, these were both identified as potentially disease-related (i.e., X-LAG) by the medical geneticist. In individual F1A, this led to a series of investigations (clinical and hormonal) from birth to monitor for the typical onset of X-LAG as a pituitary GH- and prolactin-secreting tumor [26]. While her initial hormonal profile in the neonatal period showed elevated levels of GH, IGF-1, and prolactin, this is not atypical in the very young, and over time all values became normal. The absence of clinical

evidence of X-LAG during the first 2 years of life did not rule out a later clinical presentation, and the presumptive diagnosis remained unaltered. By demonstrating on 4C-seq that the duplication did not induce the pathological neo-TAD necessary for X-LAG, this provided "functional" data to refute the original clinical diagnosis. As further follow-up has revealed no evidence of hormonal abnormalities, the duplication in F1A is now considered as an incidental finding and further endocrine investigations have been halted. The findings in family 2 provide additional evidence for neutral *GPR101* duplications. While the small duplication involving *GPR101* was identified in an abnormal fetus in family 2, a causative role of the duplication for the fetal abnormalities was uncertain. The neutrality of the duplication was underlined by the finding that the mother was an unexpected carrier and had no history or evidence of pituitary disease or overgrowth. Her experience shows that duplications affecting *GPR101* that do not lead to neo-TAD formation are associated with normal growth and fertility; this also provides further reassurance for the long-term outcomes in individual F1A.

A different scenario where the deployment of chromatin conformation capture-derived techniques proved highly beneficial in refining the molecular diagnostic process is seen in the analysis of an X-LAG phenocopy. In SC1, who shared strong clinical similarities with X-LAG, we used HiC to demonstrate an absence of neo-TAD formation at *GPR101*, thereby definitively excluding a diagnosis of X-LAG. Together, these data show how information derived from 4C-seq/HiC could be integrated into the clinical workflow when a potential diagnosis related to TAD disruption is raised. While the current study is limited to *GPR101*, similar approaches could be applied to other potential TAD-disrupting changes. These techniques are, however, labor and time intensive, and there is significant interest in the development of in silico tools to identify CNVs and SVs that impact TAD structure and crucially, to query which situations will lead to a potentially pathogenic effect. Predictive approaches have been described in studies of SVs on oncogene-containing TADs and enhancers in somatic cancer genomes [40]. More comprehensive tools have recently become available. Sánchez-Gaya and Rada-Iglesias developed the computational tool *Prediction Of STRuctural variant Effects* (POSTRE), which uses cell type specific data to generate pathogenicity scoring of the effect of SVs on TADs [41]. Currently, this model is designed to assess neurodevelopmental, neural crest, limb, and cardiovascular phenotypes, but could interrogate pituitary somatotrope phenotypes if supplemented with relevant pituitary gene expression and enhancer data sources (RNA-Seq, Chip-Seq, etc.) In the future, such in silico models could permit calling of SV effects on TADs and filter out likely benign SVs, thereby limiting the need for time-consuming chromatin capture experiments.

Prenatal genetic testing has evolved significantly over the past 20 years, moving from the use of karyotype analysis to CMA, and fetal exome sequencing in at-risk pregnancies [42, 43]. In step with these technical improvements, increasing yields have been seen in terms of pathogenic/likely pathogenic genetic variants that are related to fetal anomalies [42, 44, 45]. However, such technical innovations have been accompanied by challenges related to the calling and reporting of SNVs, CNVs, and SVs [42, 44–47]. Also, as many genetic conditions do not have visible features in the prenatal period, fetal ultrasound is often limited in its ability to predict the expected phenotype from rare genetic variants. When a genotype is diagnosed first, additional genomic technologies (e.g., methylation profiling and long-read sequencing) that provide functional evidence are critical in supporting or eliminating pathogenicity. These studies can allow for more precise prenatal genetic counseling, reduce uncertainty, and thus improve the patient's experience of prenatal diagnostic testing. The current study shows how 4C-seq/HiC can be deployed as a source of clinically relevant information on the functional implications of CNVs that potentially affect TAD borders.

Conclusions

Disruption of TADs can lead to heritable genetic diseases with a major burden on a person's overall health, as is the case in X-LAG. Determining the potential pathogenicity of CNVs/SVs on TAD structure and function can be challenging, particularly in apparently unaffected carriers. We used 4C-seq/HiC to differentiate duplications involving *GPR101* that had neutral effects on TAD structure from those that generated a neo-TAD, causing the clinical phenotype of X-LAG. Furthermore, we showed that the conservation of an invariant centromeric TAD boundary prevented ectopic enhancer adoption and the formation of a pathogenic neo-TAD. These experiences show that in emerging diseases related to TAD structure, 4C-seq/HiC can be used to distinguish neutral from pathogenic CNVs, thereby improving information for genetic counseling and decision-making.

Supplementary Information

The online version contains supplementary material available at https://doi.org/10.1186/s13073-024-01378-5.

Additional file1: Figures S1, S2, S3, S4, S5, and S6.

Acknowledgements
The authors would like to thank the individuals and families involved for their interest and patience.

Authors' contributions
AFD, GT, and MF conceived and oversaw the study, designed experiments, and wrote all versions of the manuscript. MF performed the 4C and HiC analyses, undertook statistical interpretations, and developed figures. LAD, ES, GM, VMR, AMN, MB, PF, GDS, MR, and HG collected clinical data, undertook counseling, and investigated genetic diagnoses. FRF, J-HC, and HH performed genomic analyses including aCGH, HD-aCGH, and ddPCR. DFR-B, FB, SC, PP, AL, JRL, AB, CAS, and BL oversaw genetic and clinical diagnostic investigations and edited all manuscript drafts. All authors read and approved the final manuscript.

Funding
The work was supported in part by the following funding sources: Fondazione Telethon, Italy, grant no. GGP20130 (to GT); Society for Endocrinology equipment grant (to GT); grants from the Fonds d'Investissment pour la Recherche Scientifique 2018–2022 of the Centre Hospitalier Universitaire de Liège; Intramural Research Program, *Eunice Kennedy Shriver* National Institute of Child Health and Human Development (NICHD), National Institutes of Health (NIH) Research project Z1A HD008920 (to CS, supporting FF) and National Institutes of Neurological Disorders and Stroke (NINDS, NIH) R35NS105078 (to JRL), USA. FB received funding from the Italian Ministry of Health "Ricerca Corrente" and T3-AN-14 "LifeMap" and the Italian Ministry of University and Research PRIN PNRR 2022 and PRIN 2022. The project that gave rise to these results received the support of a fellowship from "La Caixa" Foundation (ID 100010434). The fellowship code is LCF/BQ/PR22/11920006 (to MF). GT would like to acknowledge financial support by the Italian Ministry of University and Research (grant #MSCA_0000055).

Availability of data and materials
The datasets generated during this study are available at GEO, accession code GSE193114 [29] and at the Humanitas Research Hospital and Humanitas University data repository [30].

Declarations

Ethics approval and consent to participate
The study conformed to the principles of the Helsinki Declaration. Subjects were recruited under the University of Liège Ethics committee approved protocol B707201420418; or under the *Eunice Kennedy Shriver* National Institute of Child Health and Human Development, National Institutes of Health protocol 97-CH-0076 (see ClinicalTrials.gov: NCT00001595 for details), or under Project code PGR00919 of the University of L'Aquila Internal Review Board. The Institutional Review Boards of all Centers approved the study, and written informed consent was obtained from all the subjects/guardians.

Consent for publication
Written consent to publish patient-related details was obtained for all subjects.

Competing interests
AFD, FRF, AB, CAS, and GT hold a patent on GPR101 and its function (US Patent No. 10,350,273, Treatment of Hormonal Disorders of Growth). JRL has stock ownership in 23andMe and is a paid consultant for Genome International. CAS is co-founder and Director of ASTREA, a precision medicine company. The authors declare no other competing interests.

Author details
[1]Department of Endocrinology, Centre Hospitalier Universitaire de Liège, University of Liège, Liège, Belgium. [2]Department of Pediatrics, Division of Medical Genetics, McGovern Medical School, University of Texas Health Science Center (UTHealth Houston), Houston, TX, USA. [3]Memorial Hermann-Texas Medical Center, University of Texas Health Science Center at Houston, Houston, TX, USA. [4]Department of Obstetrics and Gynecology, Columbia University Irving Medical Center, New York, NY 10032, USA. [5]Department of Life, Health and Environmental Sciences, University of L'Aquila, Via Spennati N.1, L'Aquila 67010, Italy. [6]Endocrinology Unit, Fondazione IRCCS Ca' Granda Ospedale Maggiore Policlinico, Milan, Italy. [7]Department of Clinical Sciences and Community Health, University of Milan, Milan, Italy. [8]Austin Diagnostic Clinic, 2400 Cedar Bend Dr, Austin, TX 78758, USA. [9]*Eunice Kennedy Shriver* National Institute of Child Health and Human Development (NICHD), Bethesda, MD, USA. [10]Department of Molecular and Human Genetics, Baylor College of Medicine, Houston, TX, USA. [11]Department of Human Genetics, Centre Hospitalier Universitaire de Liège, University of Liège, Liège, Belgium. [12]Medical Genetics Laboratory, Policlinico Tor Vergata Hospital, Viale Oxford 81, Rome 00133, Italy. [13]Human Functional Genetics Laboratory, IRCCS San Raffaele Roma, Rome, Italy. [14]Università Telematica San Raffaele, Rome, Italy. [15]Department of Human Pathology of Adulthood and Childhood DETEV, Endocrinology Unit, University of Messina, 98125 Messina, Italy. [16]Austin Maternal Fetal Medicine, 12200 Renfert Way Ste G3, Austin, TX 78758, USA. [17]Department of Biomedical Sciences, Humanitas University, Via Rita Levi Montalcini 4, Pieve Emanuele, Milan 20072, Italy. [18]IRCCS Humanitas Research Hospital, Milan, Italy. [19]Department of Pediatrics, Baylor College of Medicine, Houston, TX, USA. [20]Human Genome Sequencing Center, Baylor College of Medicine, Houston, TX, USA. [21]Texas Children's Hospital, Houston, TX, USA. [22]Human Genetics and Precision Medicine, Institute of Molecular Biology and Biotechnology (IMBB), Foundation for Research and Technology Hellas, Heraklion, Greece. [23]ASTREA Health, Athens, Greece. [24]Department of Pathology and Cell Biology, Columbia University Irving Medical Center, New York, NY, USA. [25]Andalusian Center for Developmental Biology (CABD), Junta de Andalucia - Universidad Pablo de Olavide (UPO) - Consejo Superior de Investigaciones Cientificas (CSIC), Seville, Spain.

Received: 16 May 2024 Accepted: 23 August 2024
Published online: 13 September 2024

References

1. Ibrahim DM, Mundlos S. Three-dimensional chromatin in disease: what holds us together and what drives us apart? Curr Opin Cell Biol. 2020;64:1–9. https://doi.org/10.1016/j.ceb.2020.01.003.
2. da Costa-Nunes JA, Noordermeer D. TADs: dynamic structures to create stable regulatory functions. Curr Opin Struct Biol. 2023;81:102622. https://doi.org/10.1016/j.sbi.2023.102622.
3. Dixon JR, Selvaraj S, Yue F, Kim A, Li Y, Shen Y, et al. Topological domains in mammalian genomes identified by analysis of chromatin interactions. Nature. 2012;485:376–80. https://doi.org/10.1038/nature11082.
4. Phillips-Cremins JE, Sauria MEG, Sanyal A, Gerasimova TI, Lajoie BR, Bell JSK, et al. Architectural protein subclasses shape 3D organization of genomes during lineage commitment. Cell. 2013;153:1281–95. https://doi.org/10.1016/J.CELL.2013.04.053.
5. Lupiáñez DG, Spielmann M, Mundlos S. Breaking TADs: how alterations of chromatin domains result in disease. Trends Genet. 2016;32:225–37. https://doi.org/10.1016/J.TIG.2016.01.003.
6. Rajderkar S, Barozzi I, Zhu Y, Hu R, Zhang Y, Li B, et al. Topologically associating domain boundaries are required for normal genome function. Commun Biol. 2023;6:435. https://doi.org/10.1038/s42003-023-04819-w.
7. Franke M, Ibrahim DM, Andrey G, Schwarzer W, Heinrich V, Schöpflin R, et al. Formation of new chromatin domains determines pathogenicity of genomic duplications. Nature. 2016;538:265–9. https://doi.org/10.1038/nature19800.
8. Lupiáñez DG, Kraft K, Heinrich V, Krawitz P, Brancati F, Klopocki E, et al. Disruptions of topological chromatin domains cause pathogenic rewiring of gene-enhancer interactions. Cell. 2015;161:1012–25. https://doi.org/10.1016/j.cell.2015.04.004.
9. Matharu N, Ahituv N. Minor loops in major folds: enhancer-promoter looping, chromatin restructuring, and their association with transcriptional regulation and disease. PLoS Genet. 2015;11:e1005640. https://doi.org/10.1371/journal.pgen.1005640.
10. Xu Z, Lee DS, Chandran S, Le VT, Bump R, Yasis J, et al. Structural variants drive context dependent oncogene activation in cancer. Nature. 2022;612:564. https://doi.org/10.1038/S41586-022-05504-4.
11. de Bruijn SE, Fiorentino A, Ottaviani D, Fanucchi S, Melo US, Corral-Serrano JC, et al. Structural variants create new topological-associated domains and ectopic retinal enhancer-gene contact in dominant retinitis pigmentosa. Am J Hum Genet. 2020;107:802–14. https://doi.org/10.1016/j.ajhg.2020.09.002.
12. Kim K, Kim M, Lee AJ, Song SH, Kang JK, Eom J, et al. Spatial and clonality-resolved 3D cancer genome alterations reveal enhancer-hijacking as

a potential prognostic marker for colorectal cancer. Cell Rep 2023;42. https://doi.org/10.1016/J.CELREP.2023.112778.
13. Pagnamenta AT, Yu J, Walker S, Noble AJ, Lord J, Dutta P, et al. The impact of inversions across 33,924 families with rare disease from a national genome sequencing project. Am J Hum Genet. 2024;111:1140–64. https://doi.org/10.1016/J.AJHG.2024.04.018.
14. Andrey G, Duboule D. Genetic cold cases: lessons from solving complex congenital limb disorders. Genes Dev. 2023;37:261–76. https://doi.org/10.1101/GAD.350450.123.
15. Cova G, Glaser J, Schöpflin R, Prada-Medina CA, Ali S, Franke M, et al. Combinatorial effects on gene expression at the *Lbx1/Fgf8* locus resolve split-hand/foot malformation type 3. Nat Commun. 2023;14:1475. https://doi.org/10.1038/s41467-023-37057-z.
16. Franke M, Daly AF, Palmeira L, Tirosh A, Stigliano A, Trifan E, et al. Duplications disrupt chromatin architecture and rewire *GPR101*-enhancer communication in X-linked acrogigantism. Am J Hum Genet. 2022;109:553–70. https://doi.org/10.1016/j.ajhg.2022.02.002.
17. Trivellin G, Daly AF, Faucz FR, Yuan B, Rostomyan L, Larco DO, et al. Gigantism and acromegaly due to Xq26 microduplications and *GPR101* mutation. N Engl J Med. 2014;371:2363–74. https://doi.org/10.1056/NEJMoa1408028.
18. Abboud D, Daly AF, Dupuis N, Bahri MA, Inoue A, Chevigné A, et al. GPR101 drives growth hormone hypersecretion and gigantism in mice via constitutive activation of Gs and Gq/11. Nat Commun. 2020;11:4752. https://doi.org/10.1038/s41467-020-18500-x.
19. Costanzi S, Stahr LG, Trivellin G, Stratakis CA. GPR101: modeling a constitutively active receptor linked to X-linked acrogigantism. J Mol Graph Model 2023;127. https://doi.org/10.1016/J.JMGM.2023.108676.
20. Abboud D, Abboud C, Inoue A, Twizere J-C, Hanson J. Basal interaction of the orphan receptor GPR101 with arrestins leads to constitutive internalization. Biochem Pharmacol. 2024;220:116013. https://doi.org/10.1016/j.bcp.2023.116013.
21. Yang Z, Wang J-Y, Yang F, Zhu K-K, Wang G-P, Guan Y, et al. Structure of GPR101-Gs enables identification of ligands with rejuvenating potential. Nat Chem Biol 2023. https://doi.org/10.1038/s41589-023-01456-6
22. Trivellin G, Tirosh A, Hernández-Ramírez LC, Gupta T, Tsai-Morris CH, Faucz FR, et al. The X-linked acrogigantism-associated gene *gpr101* is a regulator of early embryonic development and growth in zebrafish. Mol Cell Endocrinol. 2021;520:111091. https://doi.org/10.1016/j.mce.2020.111091.
23. Daly AF, Yuan B, Fina F, Caberg J-H, Trivellin G, Rostomyan L, et al. Somatic mosaicism underlies X-linked acrogigantism syndrome in sporadic male subjects. Endocr Relat Cancer. 2016;23:221–33. https://doi.org/10.1530/ERC-16-0082.
24. Beckers A, Lodish MB, Trivellin G, Rostomyan L, Lee M, Faucz FR, et al. X-linked acrogigantism syndrome: clinical profile and therapeutic responses. Endocr Relat Cancer. 2015;22:353–67. https://doi.org/10.1530/ERC-15-0038.
25. Iacovazzo D, Caswell R, Bunce B, Jose S, Yuan B, Hernández-Ramírez LC, et al. Germline or somatic *GPR101* duplication leads to X-linked acrogigantism: a clinico-pathological and genetic study. Acta Neuropathol Commun. 2016;4:56. https://doi.org/10.1186/s40478-016-0328-1.
26. Wise-Oringer BK, Zanazzi GJ, Gordon RJ, Wardlaw SL, William C, Anyane-Yeboa K, et al. Familial X-linked acrogigantism: postnatal outcomes and tumor pathology in a prenatally diagnosed infant and his mother. J Clin Endocrinol Metab. 2019;104:4667–75. https://doi.org/10.1210/jc.2019-00817.
27. Naves LA, Daly AF, Dias LA, Yuan B, Zakir JCO, Barra GB, et al. Aggressive tumor growth and clinical evolution in a patient with X-linked acrogigantism syndrome. Endocrine. 2016;51:236–44. https://doi.org/10.1007/s12020-015-0804-6.
28. Grob S, Cavalli G. Technical review: a hitchhiker's guide to chromosome conformation capture. Methods Mol Biol. 2018;1675:233–46. https://doi.org/10.1007/978-1-4939-7318-7_14.
29. Trivellin G. https://www.ncbi.nlm.nih.gov/geo/query/acc.cgi?acc=GSE193114 2023.
30. Trivellin G. 4C-seq/HiC distinguishes pathogenic from neutral duplications at the *GPR101* locus: clinical application of chromatin conformation capture techniques to refine genetic diagnosis 2024. https://doi.org/10.5281/zenodo.11106834.
31. Noordermeer D, Leleu M, Schorderet P, Joye E, Chabaud F, Duboule D. Temporal dynamics and developmental memory of 3D chromatin architecture at *Hox* gene loci. Elife. 2014;3:e02557. https://doi.org/10.7554/eLife.02557.
32. Wickham H. ggplot2. Cham: Springer International Publishing; 2016. https://doi.org/10.1007/978-3-319-24277-4.
33. Rao SSP, Huntley MH, Durand NC, Stamenova EK, Bochkov ID, Robinson JT, et al. A 3D map of the human genome at kilobase resolution reveals principles of chromatin looping. Cell. 2014;159:1665–80. https://doi.org/10.1016/J.CELL.2014.11.021.
34. Franke M, De la Calle-Mustienes E, Neto A, Almuedo-Castillo M, Irastorza-Azcarate I, Acemel RD, et al. CTCF knockout in zebrafish induces alterations in regulatory landscapes and developmental gene expression. Nat Commun. 2021;12:5415. https://doi.org/10.1038/s41467-021-25604-5.
35. Li H, Durbin R. Fast and accurate short read alignment with Burrows-Wheeler transform. Bioinformatics. 2009;25:1754–60. https://doi.org/10.1093/bioinformatics/btp324.
36. Durand NC, Shamim MS, Machol I, Rao SSP, Huntley MH, Lander ES, et al. Juicer provides a one-click system for analyzing loop-resolution Hi-C experiments. Cell Syst. 2016;3:95–8. https://doi.org/10.1016/J.CELS.2016.07.002.
37. Kruse K, Hug CB, Vaquerizas JM. FAN-C: a feature-rich framework for the analysis and visualisation of chromosome conformation capture data. Genome Biol. 2020;21:303. https://doi.org/10.1186/s13059-020-02215-9.
38. Trivellin G, Faucz FR, Daly AF, Beckers A, Stratakis CA. Hereditary endocrine tumours: current state-of-the-art and research opportunities: GPR101, an orphan GPCR with roles in growth and pituitary tumorigenesis. Endocr Relat Cancer. 2020;27:T87-97. https://doi.org/10.1530/ERC-20-0025.
39. Daly AF, Beckers A. The genetic pathophysiology and clinical management of the TADopathy, X-linked acrogigantism. Endocr Rev 2024:bnae014. https://doi.org/10.1210/endrev/bnae014.
40. Xu Z, Lee DS, Chandran S, Le VT, Bump R, Yasis J, et al. Structural variants drive context-dependent oncogene activation in cancer. Nature. 2022;612(7940):564–72. https://doi.org/10.1038/s41586-022-05504-4.
41. Sánchez-Gaya V, Rada-Iglesias A. POSTRE: a tool to predict the pathological effects of human structural variants. Nucleic Acids Res. 2023;51:e54–e54. https://doi.org/10.1093/NAR/GKAD225.
42. Monaghan KG, Leach NT, Pekarek D, Prasad P, Rose NC. The use of fetal exome sequencing in prenatal diagnosis: a points to consider document of the American College of Medical Genetics and Genomics (ACMG). Genet Med. 2020;22:675–80. https://doi.org/10.1038/s41436-019-0731-7.
43. Dungan JS, Klugman S, Darilek S, Malinowski J, Akkari YM, Monaghan KG, et al. Noninvasive prenatal screening (NIPS) for fetal chromosome abnormalities in a general-risk population: an evidence-based clinical guideline of the American College of Medical Genetics and Genomics (ACMG). Genet Med. 2023;25:100336. https://doi.org/10.1016/j.gim.2022.11.004.
44. Hillman SC, McMULLAN DJ, Hall G, Togneri FS, James N, Maher EJ, et al. Use of prenatal chromosomal microarray: prospective cohort study and systematic review and meta-analysis 2013. https://doi.org/10.1002/uog.12464
45. Basel-Salmon L, Sukenik-Halevy R. Challenges in variant interpretation in prenatal exome sequencing. Eur J Med Genet. 2022;65:104410. https://doi.org/10.1016/J.EJMG.2021.104410.
46. Muys J, Blaumeiser B, Janssens K, Loobuyck P, Jacquemyn Y. Chromosomal microarray analysis in prenatal diagnosis: ethical considerations of the Belgian approach. J Med Ethics. 2020;46:104–9. https://doi.org/10.1136/MEDETHICS-2018-105186.
47. Chakravorty S, Hegde M. Inferring the effect of genomic variation in the new era of genomics. Hum Mutat. 2018;39:756–73. https://doi.org/10.1002/HUMU.23427.

Publisher's Note